

Doc 2 266

LA-8645-MS

①

124
3/4/81 T.S.

R2459

**Suitability of High-Current Standing-Wave
Linac Technology for Ultra-Relativistic
Electron Beam Propagation Experiments**

MASTER

University of California



LOS ALAMOS SCIENTIFIC LABORATORY

Post Office Box 1663 Los Alamos, New Mexico 87545

DISTRIBUTION OF THIS DOCUMENT IS UNLIMITED

DISCLAIMER
The views and conclusions contained herein are those of the author(s) and are not necessarily endorsed by the United States Government. This document is intended to provide accurate and authoritative information in regard to the subject matter covered. It is sold with the understanding that the publisher is not engaged in rendering professional service. If professional advice or other expert assistance is required, the services of a competent professional person should be sought. The copyright in this document rests with the United States Government. This document is in the public domain in the United States of America. This document is also in the public domain in the United Kingdom and other countries where the Crown Copyright Act applies.

SUITABILITY OF HIGH-CURRENT STANDING-WAVE LINAC TECHNOLOGY FOR ULTRA-RELATIVISTIC ELECTRON BEAM PROPAGATION EXPERIMENTS

by

David C. Moir, Rickey J. Faehl, Barry S. Newberger, and Lester E. Thode

ABSTRACT

Near-term development of the existing PHERMEX standing-wave linac would provide a 40-60 MeV electron beam with a current of 3 kA capable of answering a number of fundamental issues concerning endoatmospheric, ultra-relativistic electron beam propagation. Inherent high-repetition rate and multiple-pulse capability would allow alternative propagation scenerios to be investigated. Much of the theoretical expertise required to support the technology development and time-resolved beam propagation experiments presently resides within the Theoretical Applications Division.

I. INTRODUCTION

Significant interest persists, both here¹ and abroad,² in the technology development of intense charged particle beams and propagation of such beams through plasma formed in neutral gas by the beam itself. Due to the substantial source of free energy represented by the drift energy of the beam, propagation could be plagued by a variety of well-known macroinstabilities and microinstabilities, e.g. hose,³ kink,⁴ two-stream⁵⁻⁷, and filamentation.⁸⁻¹⁰

Because of the complex, time-dependent interplay between plasma generation and collective instabilities, it is essential that time-resolved propagation experiments in the 20-60 MeV be conducted to provide a baseline for theory, in order that reliable scaling laws can be established. In this regard, near-term technology development of the existing PHERMEX standing-wave linac¹¹ would provide a device for answering a number of fundamental issues concerning

EB

endoatmospheric, ultra-relativistic electron beam propagation. PHERMEX has an intrinsic high repetition rate and multiple-pulse capability, and thus a number of propagation scenerios could be investigated. Such development work, which would primarily be directed toward increasing the beam current, is consistent with the LASL weapon program and, in fact, would complement and support the present and planned development effort. Also, such development work could impact other programs of interest to directed energy research, e.g. White Horse.

PHERMEX is an acronym for Pulsed High Energy Radiographic Machine Emitting Xrays. The facility consists of a 50 MHz standing-wave linear electron beam accelerator, extensive diagnostic capability suitable for investigating complex, time-dependent physical phenomenon, and is situated in a blast-proof building at a remote, controlled access site. Within the controlled access area, a clear line of site of approximately 2000 meters exists.

At present, PHERMEX typically operates at 20-30 MeV with a peak current of 300 A. With the arrival of a new pulser for the injector, a 600-800 A beam development effort has begun. An upgrade of the amplifiers will be completed in the near future giving PHERMEX an operating range of 20-60 MeV. On the longer term, an increase in beam current to about 3 kA appears feasible, based upon initial estimates for the injector, optics, and cavity loading. Standing-wave accelerator technology has not been pushed to the high-current limit. Capabilities beyond 3 kA at this time are speculative. Better estimates as to the possibility of extending the beam current to perhaps 10 kA can be made after the 3 kA development work is complete. If 10 kA can be achieved at all, it might be possible to attain that current within a two-year time frame.

Since the facility was completed in 1963, PHERMEX has been used almost exclusively for flash radiography in the weapon and weapon-related programs. Recently, a number of experiments intended to investigate the feasibility of using PHERMEX for propagation studies were carried out. These experiments included beam characterization, time-resolved net current measurements as a function of gas pressure, and microinstability propagation experiments in which the effect of beam quality and gas pressure were investigated. From these experiments, we found the PHERMEX electron beam accelerator to be an extremely reproducible experimental device in its present configuration, and with upgraded voltage and current could provide near-term technology assessment of endoatmospheric propagation.

The theoretical support for PHERMEX technology development and extensive beam propagation research exists within the Theoretical Applications Division. In particular, a family of fully relativistic, fully electromagnetic particle-in-cell plasma simulation codes exists which have been successfully used to understand the basic physics of and produce the design for diode configurations for ultra-high current beam generation.^{12,13} The physics of transport,¹⁴ control,^{15,16} and stability¹⁷ of intense beams in vacuum has also been investigated with equal success. Code development in progress will result in the family being extended to three dimensions, with both the two- and three-dimensional codes capable of calculating aperiodic, time-dependent phenomenon in any orthogonal coordinate system. Thus, these codes represent the most powerful tool for high-current accelerator development.

Large MHD codes, Monte Carlo and atomic physics packages relevant to air chemistry calculations, and the capability to develop EMP codes suitable for passive tracking calculations also exist within the Theoretical Applications Division. Finally, a number of staff members in the Division are experts in the analytical and computational investigations of beam-plasma microinstabilities;^{6,7,18-20} this is the class of collective interactions that has been largely ignored in establishing the technology base for charged particle beams.

Section II contains a description of the PHERMEX facility. Preliminary propagation experiments are discussed in Section III. As a demonstration of the present state of particle-in-cell plasma simulation capability, an aperiodic, fully time-dependent cavity loading simulation is discussed in Section IV. Finally, a brief summary of recent, relativistically correct microinstability calculations is given in Section V.

II. PHERMEX AS AN INTENSE ELECTRON BEAM SOURCE

PHERMEX is an acronym for Pulsed High Energy Radiographic Machine Emitting X-rays. The facility consists of a 50 MHz standing-wave linear electron beam accelerator housed in a blast-proof building. The pulsed 20-30 MeV electron beam is focused on a tungsten target to produce a bremsstrahlung radiation spectrum, which is used for flash radiography of exploding systems.¹¹

The original facility was built between 1957 and 1963, and until recently has been used almost exclusively for flash radiography in weapon and weapon-related programs. Use of the PHERMEX facility for electron beam experiments

has only recently been considered. The following factors have been important in this decision:

- A. Slight reduction in the hydrodynamic shot schedule,
- B. Increased reliability of the linear accelerator,
- C. Upgrade of detection chamber fast electronics, and
- D. Interest in extending the basic physics of intense electron beams.

The PHERMEX accelerator parameters are summarized in Table I. The first column refers to the present parameters and the second to the parameters after an upgrade program which is in progress and scheduled for completion in late FY 1981. A schematic drawing of the accelerator with the important elements is shown in Fig. 1.

Electrons are generated on a hot-cathode injector. The cathode is pulsed by a high-voltage pulse and electrons are accelerated and focused into α -cavity. The present injector system consists of a 10-cm diameter sintered tungsten-barium oxide impregnated cathode which operates at 1100° C. The surface emits 6-8 A/cm². At present, the cathode is pulsed by a 600 kV Femcor pulser which determines the macroscopic time structure of the beam. Various pulse widths in Table I are attained by physically changing pulser units. The Femcor pulsers are not synchronized to the 50 MHz rf of the accelerating cavities because the time jitter of the output pulse (± 30 ns) is significantly larger than the time between two successive accelerating cycles. In addition, the risetime for both the 200 ns and 100 ns pulses is larger than the accelerating period.

The Femcor pulser will be replaced by a three pulse 1 MV system constructed by Physics International (PI). The projected increase in current is due to the increased voltage of the pulser. However, it is limited by the maximum emission capability of the hot cathode. The PI pulser is capable of generating one, two, or three pulses (each approximately 40 ns in duration) completely merged or separated by delays of up to 30 μ s. PI has tested delays between pulses up to 100 μ s and larger delays may be possible but are as yet untested. The output pulse has low jitter (± 8 ns) and a fast risetime and it will be synchronized with the 50 MHz rf.

The microscopic time structure of the beam is produced by the accelerating cycles of the 50 MHz rf which occur every 20 ns. The first cavity (α) acts as

TABLE I
SUMMARY OF PRESENT AND POST-UPGRADE PHERMEX ACCELERATOR PARAMETERS

INJECTOR (HOT CATHODE)	<u>Today</u>	<u>Post-Upgrade</u>
Voltage (MV)	0.550	1.00-1.25
Current (A)	350	650
Pulse Width (ns)	200, 100, 40	150, 80, 40
Risetime (ns)	50, 40, 15	13, 13, 13
RF Synchronized	No	Yes
Emittance (mm-mrad)	$< 500 \pi$	$< 500 \pi$
Spotsize (mm)	25	25
RF CAVITIES		
Frequency (MHz)	50	50
Length (m)	2.6	2.6
Diameter (m)	4.6	4.6
Field Strength (MV/m)		
α	3.6	12.0
β	5.5	10.0
γ	3.4	8.0
Stored Energy (J)		
α	610	6800
β	1430	4700
γ	550	3000
Energy Depletion (α -cavity)		
One Micropulse	6%	3%
Ten Micropulses	30%	20%

a chopper and accelerator with substantial stored energy depletion in that cavity. The micropulses generated by rf acceleration are approximately gaussian with a 3.3 ns FWHM. The number and amplitude of the micropulses in a macropulse is clearly dependent on the injected pulse shape and timing relative to the rf. Figure 2 is a time resolved measurement of the electron beam current for a 200 ns pulse on the injector from the Femcor pulser. Note that a sub-burst with maximum current does not occur until the third pulse. This

phenomena is a function of pulse risetime and jitter relative to the rf. At present, the initial conditions for a full amplitude pulse are unknown and determined by the initial low intensity pulses. Installation of the PI 1-MV pulser, which will be synchronized with the rf, will yield an initial sub-burst of full amplitude. This upgrade is significant for electron beam experiments.

PHERMEX has three rf cavities shown schematically in Fig. 1. These are designated α , β , and γ . The beam is injected into α . The field strength in the cavities is generated by rf amplifiers. As part of the upgrade, the existing amplifiers are being replaced with amplifiers of higher power. As a consequence, the field strengths and stored energy in the cavities will be greatly increased.

Electron beam energy is determined by the strength of the cavity fields. The beam energy and other output beam parameters are summarized in Table II. Beam energy dispersion and emittance have been determined by calculation using beam spot size measurements at two locations in the drift space, a field map of the final focusing lens, and the beam spot size at the focus.

As noted earlier, the time structure of the output beam is determined macroscopically by the injection pulse and microscopically by the 50 MHz rf. These parameters are also summarized in Table II.

Figure 3 is a glass plate measurement of the PHERMEX electron beam distribution at the focus. The white spot is due to a threshold effect in the radiation damage of the glass plate. The diameter of the white spot is assumed to be the beam spot size. However, radiographic techniques used to determine beam spot size indicate a slightly smaller value.

The beam current measurement, shown in Fig. 2, and spot size, indicated in Fig. 3, can be combined to determine the peak current density and electron density in individual micropulses. These values are also summarized in Table II. It should be noted again that these values are for a single micropulse of maximum amplitude.

As also noted earlier, the support electronics associated with PHERMEX have been upgraded. This upgrade substantially enhances our capability to perform time-resolved electron beam experiments. Table III is a summary of the presently available electronics. This particular phase of the upgrade program is essentially complete.

It is useful to compare PHERMEX with other machines in terms of relativistic factor γ , current, current density, pulse duration and total beam energy.

TABLE II
SUMMARY OF PRESENT AND POST-UPGRADE PHERMEX ELECTRON BEAM PARAMETERS

	<u>Today</u>	<u>Post-Upgrade</u>
MEAN ENERGY (MeV)	21	40
ACCESSIBLE ENERGY RANGE (MeV)	20-30	20-60
ENERGY DISPERSION	4%	4%
EMITTANCE (mm-mrad)	7 π	7 π
TIME STRUCTURE		
Macropulse Width (ns)	200, 100, or 40	150, 90, or 40
Risetime (ns)	51, 37, 15	13, 13, 13
Number of Micropulses	10, 5, 2	7, 4, 2
Micropulse Width (ns)	3.3 (FWHM)	3.3 (FWHM)
INTENSITY		
Average over Macropulse (A)	50 (200 ns)	90 (150 ns)
Peak (kA)	0.30	0.60-0.80
Electrons/Micropulse	6×10^{12}	1.2×10^{13}
Current Density (Peak) (A/m ²)	4×10^8	8×10^8
Electron Density (Peak) (e/m ³)	4×10^{18}	8×10^{18}
SPOT SIZE (DIAMETER)		
Exit of Collimating Lens (mm)	15	15
Entrance to Focusing Lense (mm)	10	10
On Target with 0.5 m Focus (mm)	≤ 1	≤ 1

TABLE III
SUMMARY OF AVAILABLE ELECTRONICS ASSOCIATED WITH PHERMEX FACILITY

COMPUTER

Data General, 80 k Memory, 10 M byte disc, 9 track tape unit,
floppy disc, Versatech printer, 2-Camac crates.

TRANSIENT ANALYZERS

Tektronix R-7912, 11 channels, 250 MHz bandwidth
Biomation 8100, 6 channels, 25 MHz bandwidth
Tektronix Oscilloscopes, 5, 50 MHz bandwidth

TIMING CHANNELS

Nanofast, 20 channels, 0.1 ns resolution, ± 1 ns accuracy,
200 μ s total range
Nanofast, 10 channels, 10.0 ns resolution, ± 10 ns accuracy,
10 s total range

TABLE IV
COMPARISON OF PHERMEX ACCELERATOR WITH OTHER ELECTRON BEAM
GENERATORS AND ACCELERATORS

	γ	I (kA)	J (kA/cm ²)	τ (ns)	U (J)
FX-25	2.9	15.0	4.8	30.0	600
PI 1590	13.0	100.0	15.0	60.0	40000
ASTRON	7.8	0.10	0.13	300	120
ETA	4.8	10.0	60	30.0	1500
PHERMEX	41	0.30	40	3.3	200*
PHERMEX (post-upgrade)	41-121	0.60-0.80+	80	3.3	280-1130*
ATA	98	10.0	60	30	15000

γ = electron energy/electron rest mass

I = electron beam current

J = current density (peak)

τ = pulse length of individual pulses

U = total beam energy (U = IV τ x number of micropulses)

* PHERMEX generates multiple pulses

+ present development effort

This comparison is given in Table IV. At present, PHERMEX is the only high γ machine in operation. The current density is sufficiently high that beam-plasma effects are important. However, the peak current and total energy are somewhat low in comparison with what is considered optimum for beam propagation. On the other hand, with 3 kA of beam current, combined with the existing multiple pulse capability, PHERMEX would represent a powerful and versatile device for investigating ultrarelativistic, endoatmospheric beam propagation.

III. PRELIMINARY PROPAGATION EXPERIMENTS

In order to demonstrate the feasibility of using PHERMEX as an intense electron beam source, some beam characterization and preliminary propagation experiments were performed.

Figure 4 is a drawing of the basic experimental arrangement for all of the electron beam studies. All experiments were performed external to the building on the PHERMEX firing point. The electron beam is focused through a tapered beryllium collimator, and exits through a 0.25-mm thick beryllium window. A new section of drift tube was inserted through the existing accelerator bull-nose from the outside. This new drift tube contains a 1.3×10^{-2} mm kapton vacuum window, which is located 7 mm from the beryllium window. Thus, a 7 mm air gap, which has a negligible effect on the beam, exists between the two drift spaces. For this configuration, the position of the 1 mm diameter beam focus is located about in the center of the air gap.

Initial experiments were directed toward characterizing the PHERMEX electron beam. The first experiment was a time-resolved current measurement in vacuum using a graphite charge collector located 50 cm from the 1 mm focus. The results of this experiment are shown in Fig. 2 and were discussed in Section I.

In an attempt to further unfold the beam distribution function, the beam momentum scatter was varied by placing additional scattering foils in the gap between the beryllium and kapton vacuum windows. High-resolution glass photographic plates (Kodak S0343) were then used to measure the beam spatial distribution at 60 cm from the beam focus. For propagation in vacuum, the densitometer scans of the beam spatial distribution for various added scattering materials are shown in Fig. 5. As expected, the increased beam scatter produced a measurable, systematic change in the spatial distribution function. To zero

order, the particle trajectories are ballistic because the PHERMEX beam has a $v/\gamma \sim 3.8 \times 10^{-4}$. Here, we use conventional notation: $v = Nr_e$, where N is the number of the beam electrons per unit length, r_e is the classical electron radius, and γ is the relativistic factor. For the photographic plate data, the integrals of the distributions are normalized to be the same.

In Fig. 6, the beam divergence calculated on the basis of the beam spatial distribution, with systematic beam divergence subtracted out, is compared with what would be predicted by Molière multiple scattering theory.²¹ The experimental errors are dominated by the uncertainty in the systematic beam divergence, which has been calculated to be about $\theta_{div} \sim 20$ mrad. However, the systematic divergence has not been measured directly. From these data, the random angular scatter in the beam momentum distribution is in good agreement with theory.

The beam distributions in Fig. 5 show no evidence of structure. From this result and spot size at the focus, an estimate of the co-linearity of the micropulses can be derived. Spatially, the micropulses are separated by less than 1 mm at the focus. The maximum angular separation is less than 5 milliradians.

The first set of time integrated data was beam distribution measurements normal to the PHERMEX beam. The detectors for these measurements were glass plates. They were positioned 60 cm from the 1 mm focus. Figures 7a and 7b are a compilation of the results. The plates are arranged as a function of nitrogen gas pressure (row) and increasing beam scatter (column). The distribution indicates that beam instabilities are present and decrease with both increasing beam scatter and gas pressure at a position 60 cm from the beam focus.

Open shutter photographs were made of the beam propagating through neon and helium. A lucite drift tube was attached to the end of the metal drift tube, as shown in Fig. 4. Figures 8a and 8b contain the results of measurement for neon and helium, respectively. The beam is propagating from left to right with the extreme left being located 60 cm from the focus. The results at low pressure for both gases show the possible existence of a two-stream instability. This is evidenced by the bright glow of the gas near the entrance into the lucite drift tube. At higher pressures, the beam is breaking up into filaments. The transverse distribution is consistent with what is seen in the normal distributions measured by glass plates. To verify that these effects

were not produced by discontinuities in the return-current path, open shutter photographs were made with the lucite drift tube lined with copper wire screen. The photographs indicated that the return-current discontinuity had no visible effect.

To understand the effect of the beam microstructure, time-resolved measurements were made of the beam propagating in neon and helium. Time resolved measurements of the normal and transverse beam distribution were made using an IMACON 790 fast-frame/streak camera. The camera was able to record a 10 ns frame every 50 ns. Figure 9 is a reproduction of normal beam distribution for a beam propagating in 3 torr of neon. The numbered overlay relates the images to appropriate beam micropulses. Cherenkov light produced by electrons passing through a thin plastic sheet was used to generate light for the images. It is located 1.9 m from the focus. Synchronization of the camera relative to the micropulses was determined using the NanoFast time digitizer and is shown in the schematic below the picture. Photographs were also taken of the transverse beam distribution where the light was generated by the gas itself. The following conclusions can be reached from these measurements: (1) the micropulses propagate independently, and (2) there is no light emitted from the gas during the 20 ns between pulses. Note, however, that no ultra-violet light is transmitted through the lucite drift tube.

A segment of the metal drift tube was constructed which contained magnetic-field (B) probes. It was attached to the end of the drift tube used in previous experiments. Figure 10 is a photograph of this section. A kapton window was placed on the downstream end. The charge collector was attached to the end of the drift tube. Figure 11 is a diagram of the entire arrangement. The charge collector was maintained at vacuum, and the return-current probes were located in a region of variable pressure. The purpose of this arrangement was to isolate the charge collector from any electron plasma currents which might be produced in the gas by the electron beam and impinge on the charge collector.

The drift tube contained a bellows on the upstream end. This was used to align the beam on the center of the drift-tube axis. The drift tube and the charge collector were maintained at vacuum, and each of the beam probes was checked using separate beam pulses. The resulting integrated signals agree to within two standard deviations of the observed pulse-to-pulse dispersion of beam current. Probe signals were connected to a passive adder which summed the

outputs and generated a signal that was proportional to the net current traveling through the spool containing the probes.

A series of measurements was made of the net current in the gas versus the total current in the charge collector for both neon and helium. Figure 12a is a measurement of the integrated probe output for the beam propagating in vacuum. Figure 12b is the same measurement with the beam propagating through 10 μ of helium. This result indicates that after seven micropulses, the gas is sufficiently ionized that the return-current is now in the beam-generated plasma and no longer in the drift-tube wall. Figure 12c is for 1 atmosphere of helium, and the measured probe return currents which are again in the drift tube as in the vacuum case. However, the slopes are substantially different. For the first pulse, the net current is substantially larger than the actual beam current as measured by the charge collector. It is speculated that this additional current is produced by beam-generated delta rays. Figure 13 is a plot of the ratio of the net current measured by the probes to the total current measured by the charge collector as a function of pressure from vacuum to 580 torr. Between 1.0 and 10.0 torr, the net current measured by the probes is zero, and all of the return current is in the beam-generated plasma. At lower pressures (<1 torr), there is insufficient gas to generate enough plasma to conduct the entire return current. At higher pressure (>10 torr), the electrons from the ionized gas tend to rapidly recombine, thus limiting the conductivity and forcing the return current through the drift tube. The data for neon have similar properties; however, the two curves diverge in the 100-600 torr range with the neon return current being systematically lower. Unfortunately, the data cannot be systematically analyzed using the initial micropulse because the slow risetime and time jitter of the pulser yield initial pulses of varying amplitude.

IV. PRELIMINARY SIMULATION STUDIES OF ACCELERATOR CAVITY LOADING

We have undertaken numerical studies to examine dynamical cavity loading in configurations similar to those found in rf-linacs at LASL. These were preliminary and exploratory studies, representing the first attempts to our knowledge to model accelerator physics in two-dimensional, fully electromagnetic particle-in-cell (PIC) simulations. The CCUBE code, which has been described previously,¹⁴ solves Maxwell's equations on a fixed mesh and

constructs source terms by averaging the self-consistent trajectories of a large number of "particles" onto this mesh. For these studies the primary sources were the micropulses of accelerated electrons.

The accelerated particles were relativistic electrons. With an injection energy of 2.3 MeV ($\gamma_0 = 5.5$), changes in velocity were minimal during the acceleration phase. Pulses of 0.4 nsec duration were injected with a parabolic current form. Peak current on these pulses was 1.0 kA. A uniform 4.0 kG solenoidal field was imposed to transport the beam. This is in contrast to conventional accelerator transport schemes which rely on strong focusing. In the present approach, laminarity is maintained by injecting the pulses in nearly an intense beam equilibrium state. Fine tuning of the guide fields throughout the cavity can probably be used to reduce multi-cavity emittance growth. Even though these initial studies were not optimized, it should be noted that this system will easily accommodate 10 kA peak currents and more.

Excitation of the TM mode was accomplished by driving a z-slotted antenna. (This antenna was the mathematical idealization of an array of linear antennas such that $E_z = 0$ on the array, E_θ was unaffected, and the total array had no azimuthal gradients.) Cavity fields were thus rung up in a realistic fashion. This self-consistent excitation was felt to be necessary to model fringing fields in the drift tube on axis.

The fundamental TM mode has no axial gradients. The cavity could therefore be made as long as desired. Figure 14 shows the superposition of four radial profiles of the cavity field at different axial positions. A length was chosen so that significant energy transfer occurred in one transit time. Peak fields were large enough so that maximum energy extraction would be 0.85 MeV/cavity. Because the relativistic electron transit was a significant fraction of the period, $\Delta T/T = 0.2$, where $T = 2\pi/\omega$, a significant variation of accelerating gradient was sampled. Of course, this would be undesirable in an accelerator, but our goal was to maximize loading effects.

Two calculations were conducted to determine loading effects. In the first calculation, the electrons were injected to be in phase with the accelerating gradient. The other calculation involved pulses in phase with the decelerating gradient, that is 180° out of phase with first. In theory this latter operation could enhance the cavity fields, since energy is given from the electrons to the field. This will be discussed in more detail later, but suffice it to say for now that it, in fact, behaved as expected.

By taking one-half the difference between corresponding probe signals, one may gain a fairly accurate picture of the cavity loading. After transit of the first beam pulse, measurable field differences were found, out to radii of the order of the cavity length. This suggests that the radial cavity loading effects are limited primarily by speed of light propagation. This is not conclusive on the basis of one configuration. Furthermore, after multiple pulses had been accelerated, field differences were measurable at all radii.

Another interesting feature of these calculations was the perturbation of the cavity fields by the beam(s). Figure 14 showed the fundamental mode excitation with no nulls in the absence of beam. After injection, however, higher order fields were clearly evident. Figure 15 shows a similar ensemble of profiles as in Fig. 14. Third and fourth order cavity modes have been induced. This phenomena was evident in both accelerating and decelerating calculations. Emittance growth could be associated with these unwanted modes.

Preliminary studies of cavity loading indicate that short-term loading may be limited to a radial distance equal to the length of the cavity mouth. These effects are distributed over the entire cavity after several field cycles, however. Emphasis should be placed on the tentative nature of the results at present. Additional calculations with minor variation in parameters would greatly reduce uncertainties here. Even with these caveats, the simulations proved to be fruitful and illuminating. Operation of the cavities in an auto-accelerator mode, for instance, seems promising enough to warrant more detailed investigations. A trial calculation with a quasi-cw beam at 10 kA showed no net field depletion. If switching techniques are feasible, it may be possible to accelerate much higher beam currents in rf linacs than has previously been thought practical. Another unexpected bonus from the calculations was observation of extraneous mode excitation induced by these high-current beams. Overall, these calculations appear to have only scratched the surface of a much larger body of accelerator problems to which this type of sophisticated simulation coupled with analytical calculations can make significant contributions.

V. MICROINSTABILITY AND BEAM PROPAGATION

We have recently carried out an investigation of the two-stream instability in propagating beam-plasma systems. It had long been known that this

microinstability could be stabilized if the background plasma were sufficiently collisional and if the beam was comprised of particles with a distribution in velocities. This result was obtained theoretically in the nonrelativistic case,²² and phenomenological arguments were adopted by subsequent researchers to extend these results to a relativistic beam.²³ In order to place these models in their proper context, a rigorous, fully-relativistic treatment of the linear theory of two-stream instability in a collisional plasma was undertaken. Reports detailing some of the component parts comprising this theory are given in Refs. 6, 7, and 24. The relativistic dynamics complicate the physics considerably and are essentially responsible for the differences between ours and other models that are, in fact, nonrelativistic.

The theory confirms that the phenomenological models are overly optimistic with regard to mode stabilization for highly relativistic electron beams. Furthermore, for mildly relativistic beams, the phenomenological model and the more rigorous theories are in rough agreement and, hence, experiments done to date would be expected to give rise to false confidence in the phenomenological models. The linear theory also indicates that the stability criteria depend sensitively on the background plasma parameters, particularly the collision rate. In configurations where the plasma is produced by the beam itself, this quantity is likely to be time varying and not well known. This complicates experimental tests of theory, and the demand for carefully performed experiments with beam particle energy in the 20-60 MeV regime now appears essential.

The beam energy loss due to two-stream instabilities can be calculated once the phase velocities, linear frequencies, and growth rates are known. Upper-bound estimates have been made based on currently available nonlinear models,¹⁹ and these indicate, for ultra-relativistic electron beams that are linearly unstable, the nonlinear states are relatively weak. However, the effect of such weak nonlinear states on beams that are required to propagate over finite distances is an open question.

The two-stream mode is only one of many possible instability mechanisms that can plague a beam-plasma system. Experimental evidence from the preliminary PHERMEX propagation studies indicates that an electromagnetic mode of instability appears at about the point when collisions are strong enough to weaken or stabilize the two-stream mode. This is consistent with some theoretical results that are essentially nonrelativistic,¹⁰ and we have begun to extend our models²⁰ used in the two-stream theory to address this issue.

Experiments at low currents will be adequate to test the simplest theoretical models. Ultimately, the theory must be generalized to include the effect of the beam self-magnetic field. To test this theory, the beam current in an experiment must be high enough to make the betatron wavelength substantially smaller than the experimental chamber length. An experimental test in this regime is important in that it is likely that the stabilization of the mode will only come about through the action of beam self-field and finite geometry. Furthermore, it is in this regime that a meaningful comparison of growth rate with that of, for example, the hose can be made.

REFERENCES

1. "Particle Beams, Laser Weapons-1." Aviation Week & Space Technology, (July 28, 1980), 32-42.
2. "Soviets Build Directed-Energy Weapon," Aviation Week & Space Technology, (July 28, 1980), 47-50.
3. Edward P. Lee, "Resistive Hose Instability of a Beam with the Bennett Profile," Phys. Fluids 21, 1327 (1978).
4. Edward P. Lee, "Low-Frequency Hydromagnetic Kink Mode of a Relativistic Beam," Phys. Fluids 16, 1072 (1973).
5. M. M. Shoucri and A. B. Kitsenko, "Oscillations of Bounded Beam-Plasma Systems in a Cylindrical Geometry," Plasma Physics 10, 699 (1968).
6. B. S. Newberger, "Relativistic Electron Beam Propagation: Two-Stream Theory January 1978-January 1979," Los Alamos Scientific Laboratory Report LA-7912-MS (July 1979).
7. B. S. Newberger and L. E. Thode, "Two-Stream Instability for a Scattered Beam Propagating in a Collisional Plasma," Proceedings of Third International Conference on High-Power Electron and Ion Beam Research and Technology, Novosibirsk, USSR (July 1979).
8. R. Lee and M. Lampe, "Electromagnetic Instabilities, Filamentation, and Focusing of Relativistic Electron Beams," Phys. Rev. Lett. 31, 1390 (1973).
9. K. Molvig, C. W. Roberson, and T. Tajima, "Surface Filamentation of Relativistic Electron Beam in a Plasma," Phys. Fluids 21, 975 (1978).
10. T. Okada and K. Niu, "Collisional Effects in the Electromagnetic Instability for a Relativistic Electron Beam Penetrating a Plasma," Institute of Plasma Physics Report IPPJ-439, Nagoya University, Japan (February 1980).

11. D. Venable, D. O. Dickman, J. N. Hardwick, E. D. Bush, Jr., R. W. Taylor, T. J. Boyd, J. R. Ruhe, E. J. Schneider, B. T. Rogers, and H. G. Worstell, "PHERMEX: A Pulsed High-Energy Radiographic Machine Emitting X-Rays," Los Alamos Scientific Laboratory Report LA-3241 (May 1967).
12. M. E. Jones and L. E. Thode, "Intense Annular Relativistic Electron Beam Generation in Foilless Diodes," to be published in Appl. Phys. (October 1980).
13. M. A. Mostrom, "Influence of Nonuniform External Magnetic Fields and Anode-Cathode Shaping on Magnetic Insulation in Coaxial Transmission Lines," Proceedings of the Second IEEE International Pulsed Power Conference, Lubbock, Texas (June 1979).
14. L. E. Thode, B. B. Godfrey, and W. R. Shanahan, "Vacuum Propagation of Solid Relativistic Electron Beams," Phys. Fluids 22, 747 (1979).
15. R. J. Faehl, W. R. Shanahan, and B. B. Godfrey, "Simulation of Collective-Ion Acceleration in a Slow Cyclotron Beam Mode," proceedings of Third International Topical Conference on High-Power Electron and Ion Beam Research Technology (Novosibirsk, USSR, 1979).
16. W. R. Shanahan, R. J. Faehl, and B. B. Godfrey, "A Computational Study of One Aspect of Autoresonant Acceleration," IEEE Trans. Nucl. Sci., NS-26, 4226 (1979).
17. M. E. Jones and M. A. Mostrom, "The Diocotron Instability in Annular Relativistic Electron Beams," submitted to Phys. Rev. Lett.
18. L. E. Thode, "Plasma Heating by Scattered Relativistic Electron Beams: Correlations Among Experiments, Simulation, and Theory," Phys. Fluids 19, 831 (1976).
19. L. E. Thode, "Effect of Electron-Ion Collisions on the Nonlinear State of the Relativistic Two-Stream Instability," Phys. Fluids 20, 2121 (1977).
20. L. E. Thode, J. R. Cary, M. E. Jones, M. A. Mostrom, and B. S. Newberger, "Interplay Between the Two-Stream and Filamentation Instability in Ultra-Relativistic, Electron Beam Propagation," in preparation.
21. H. A. Bethe, "Molière's Theory of Multiple Scattering," Phys. Rev. 89, 1256 (1953).
22. H. E. Singhaus, "Beam-Temperature Effects on the Electrostatic Instability for an Electron Beam Penetrating a Plasma," Phys. Fluids 7, 1534 (1964).
23. R. Briggs, J. Clark, T. Fessenden, E. Lee, and E. Lauer, "Stable Propagation of a High-Current Electron Beam: Experimental Observations and Computational Modeling," Lawrence Livermore Laboratory Report UCID-17516 (1977).

24. B. S. Newberger and L. E. Thode, "A Nonlinear Two-Stream Interaction Between a Cold, Relativistic Electron Beam and a Collisional Plasma-Astron Experiment," Los Alamos Scientific Laboratory Report LA-7814-MS (May 1979).

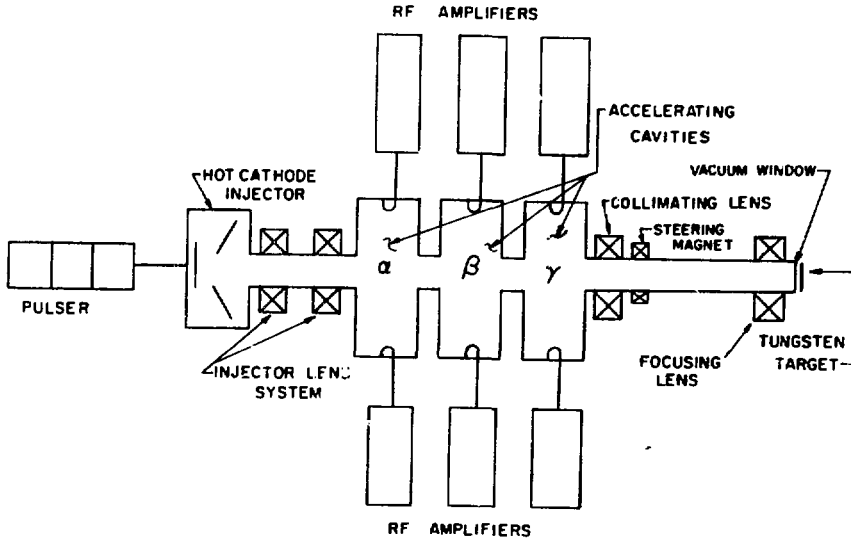


Fig. 1.

Schematic diagram depicting the important elements of the PHERMEX standing-wave linear accelerator.

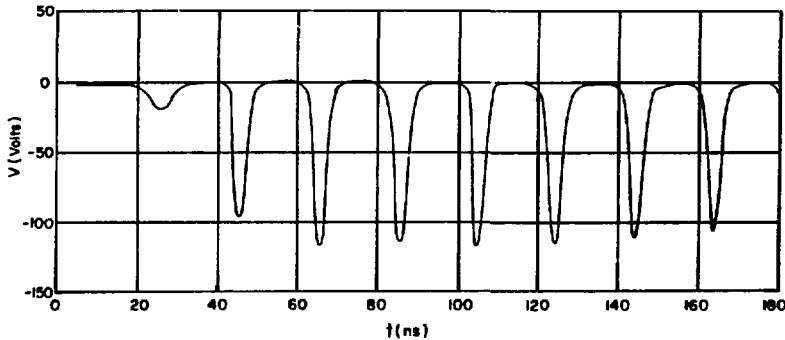


Fig. 2.

Charge-collector voltage versus time for the PHERMEX electron beam measured at 50 cm downstream of the 1 mm focus. Peak (negative) voltages correspond to 0.27 kA of current.

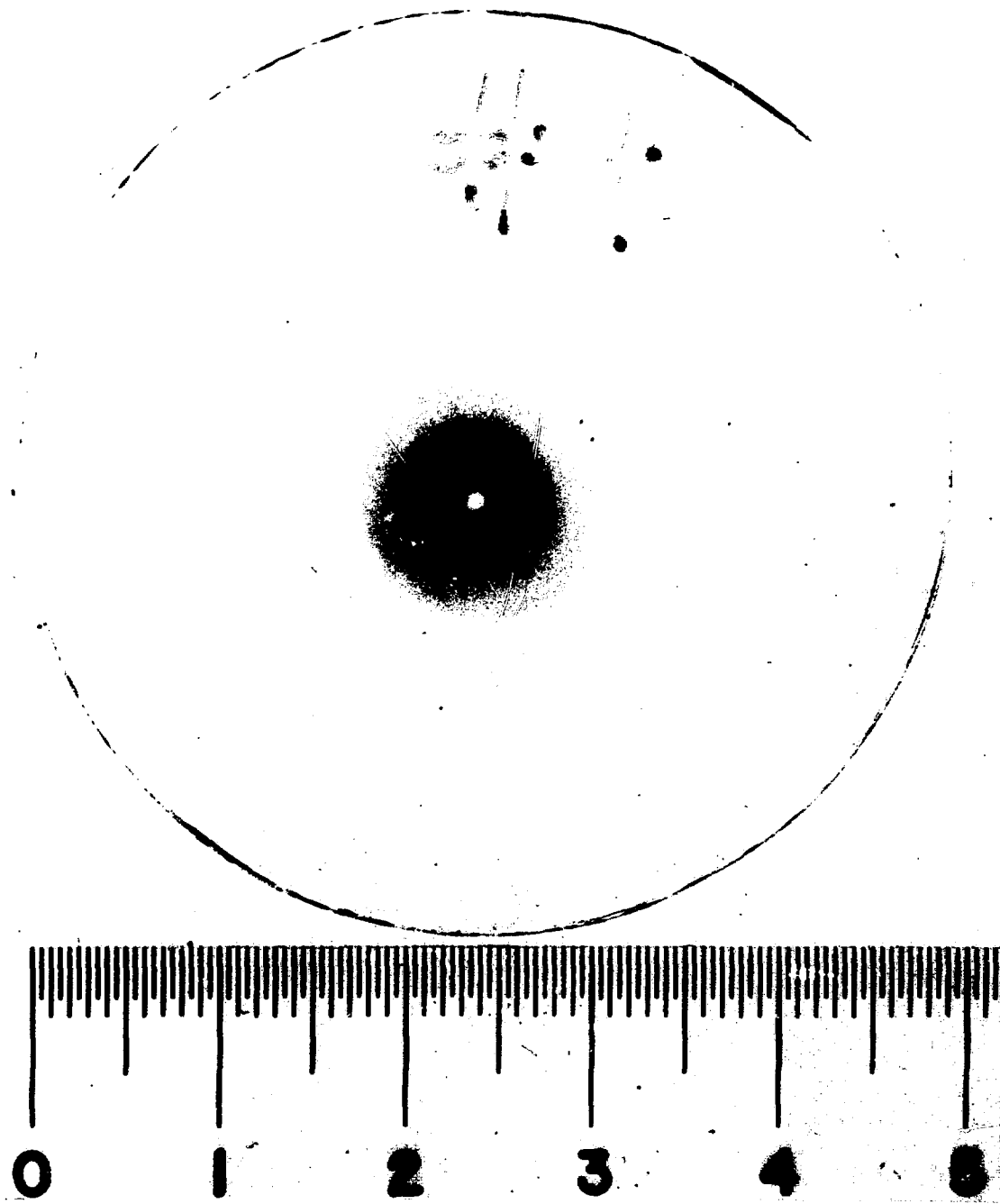


Fig. 3.

Photograph of a radiation-damaged glass plate located at the focus of the PHERMEX beam relative to centimeter scale. The white spot is due to a threshold effect in the radiation damage process.

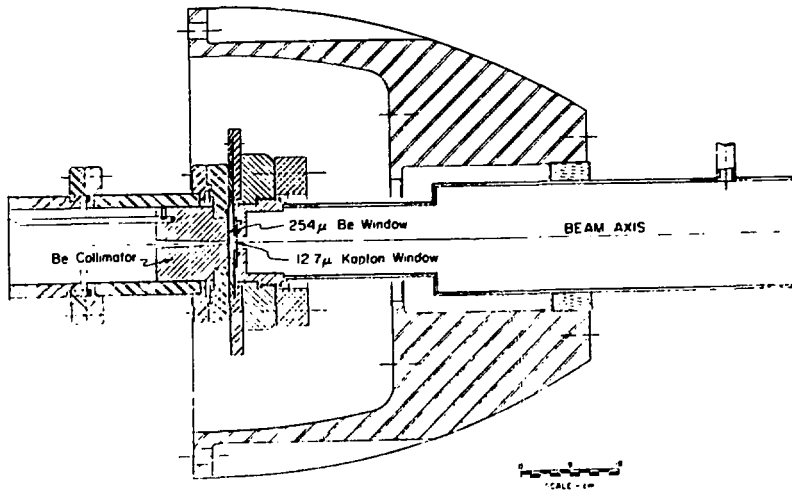


Fig. 4.

Electron beam experimental arrangement and PHERMEX bullnose. The beam is focused through the beryllium collimator to a 1-mm-diameter spot between the beryllium vacuum window and kapton window.

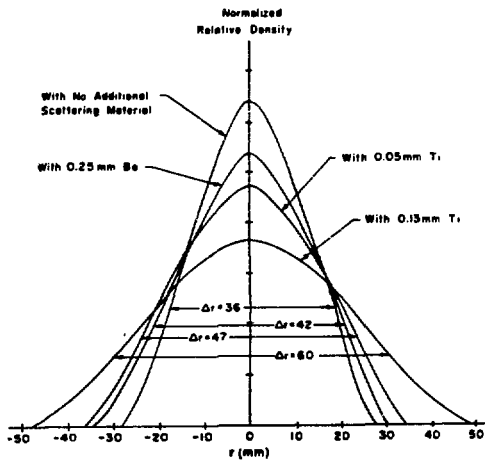


Fig. 5.

Densitometer scans of the radiation damage spot produced in glass by the beam at 60 cm from the 1 mm focus. The curves are normalized to unit area. The beam is transported in vacuum from the focus after passing through thin foils of different material and thickness, as illustrated. The respective rms diameter is also shown.

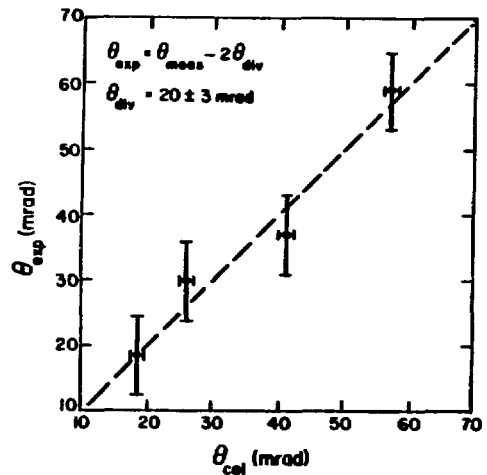


Fig. 6.

Experimentally determined mean scattering angles as a function of the calculated values from small angle multiple scattering theory. The dashed curve is $\theta_{\text{exp}} - \theta_{\text{cal}}$. The vertical error bars denote the uncertainty in the inherent beam divergence θ_{div} , while the horizontal error bars denote limits in the range of approximations in the theory.

C = No Added Material

A = +10mil Be

B = +20mil Be

E = +2mil Ti

D = +5mil Ti

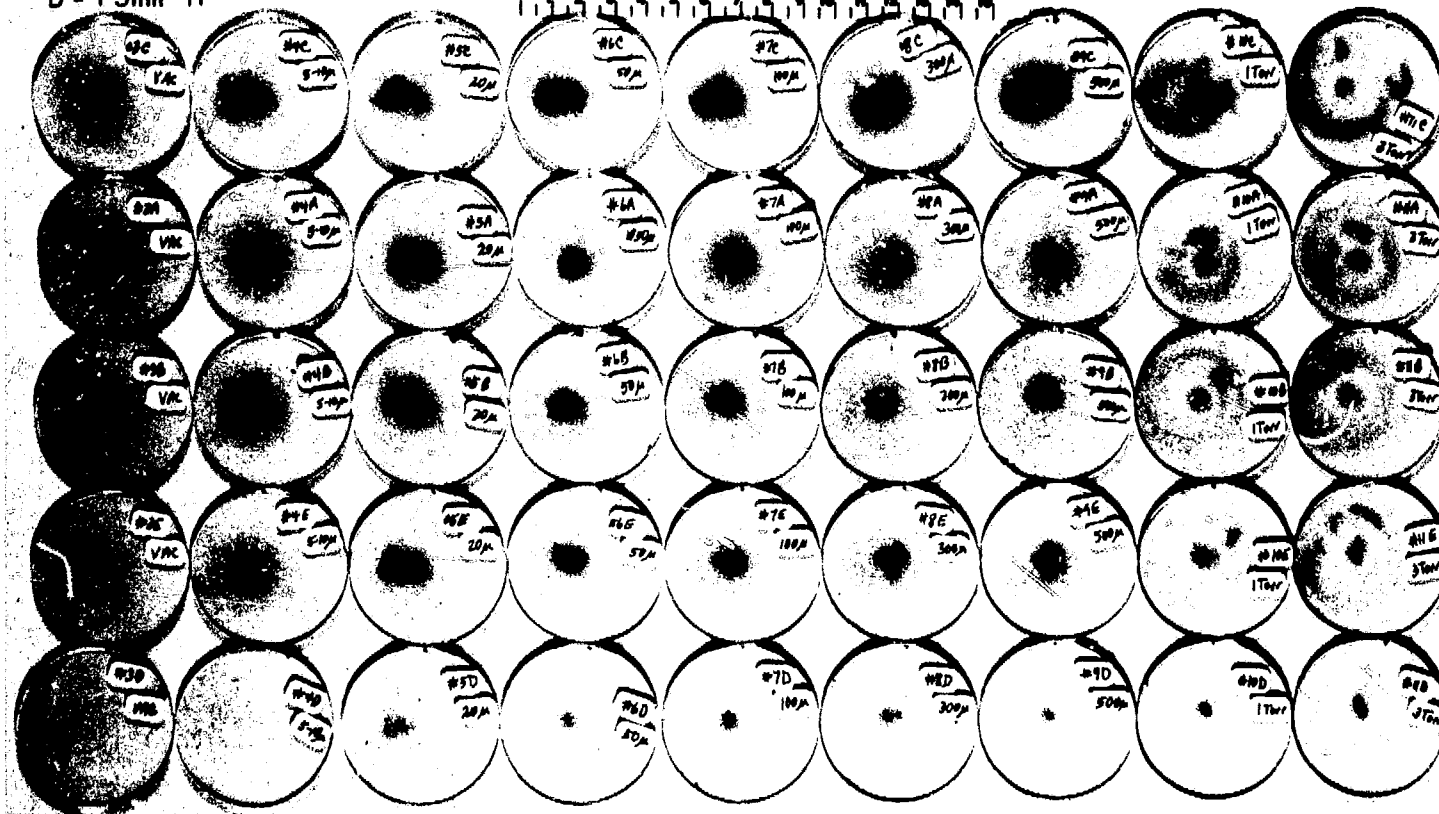


Fig. 7a.

Photographs of radiation-damaged glass plates for different values of ambient nitrogen gas pressures (horizontal) and beam scatter (vertical). Gas pressures are as indicated. Scattering angles are, from top to bottom, 18, 30, 32, 37, and 59 mrad, respectively.

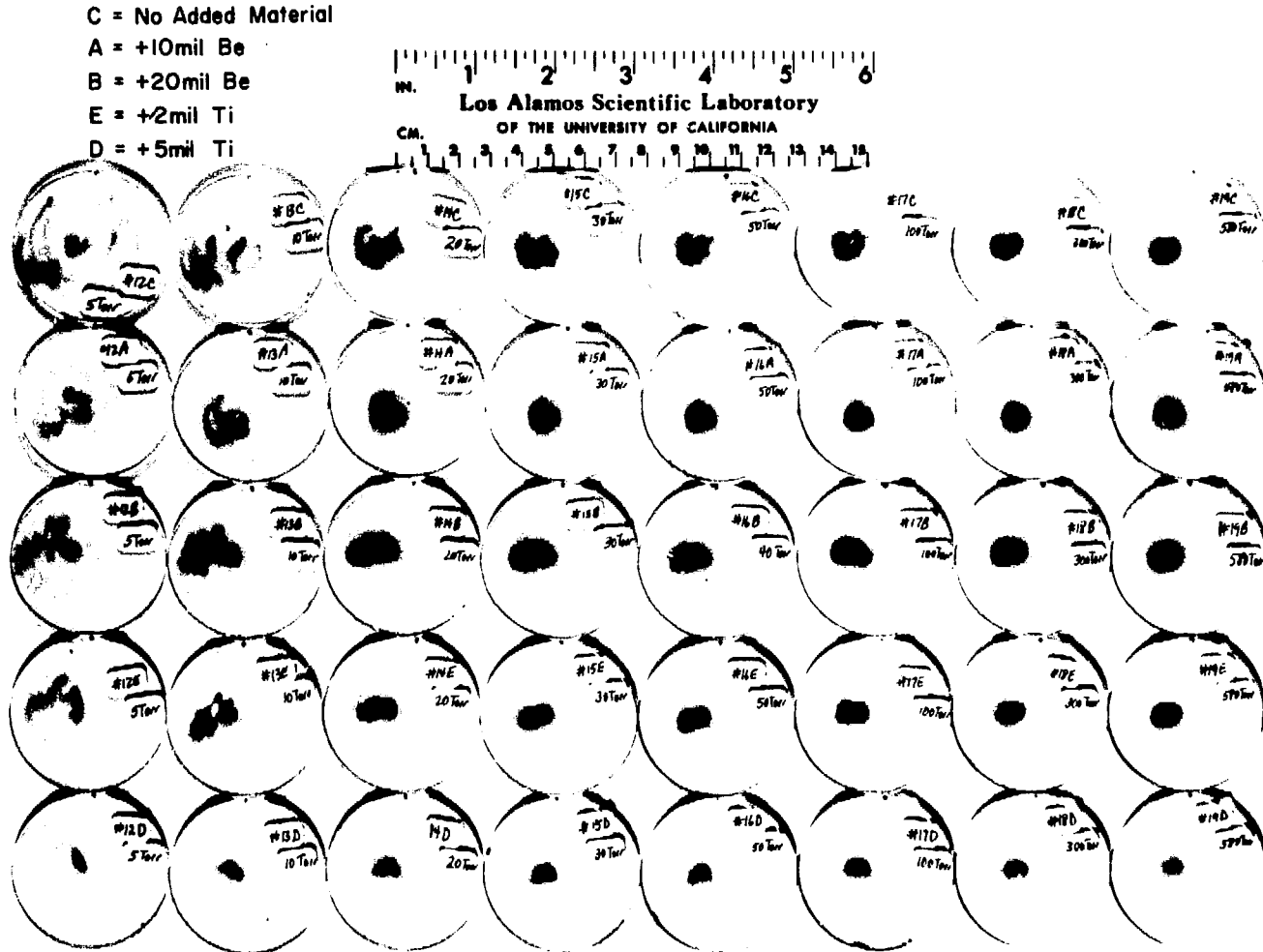


Fig. 7b.

Photographs of radiation-damaged glass plates for different values of ambient nitrogen gas pressure (horizontal) and beam scatter (vertical). Gas pressures are as indicated. Scattering angles are, from top to bottom, 18, 30, 32, 37, and 59 mrad, respectively.

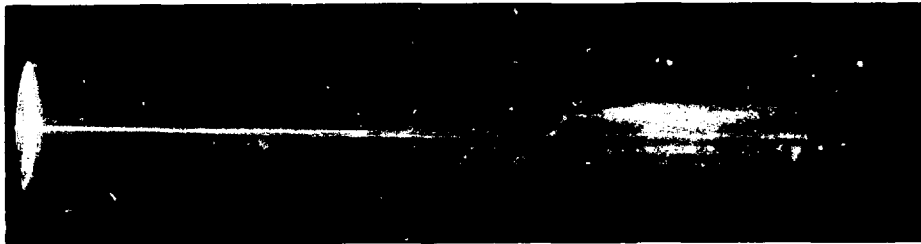
NEON



0.3 Torr



3 Torr



30 Torr



300 Torr

Fig. 8a.

Composite of open-shutter photographs of the PHERMEX beam injected into neon. The lucite drift tube begins 60 cm from the 1 mm focus, and the fiducials are 15 cm apart. The blue glow is Cherenkov light in the lucite.

HELIUM



1 Torr



3 Torr



30 Torr



300 Torr

Fig. 8b.

Composite of open-shutter photographs of the PHERMEX beam injected into helium. The lucite drift tube begins 60 cm from the 1 mm focus, and the fiducials are 15 cm apart. The blue glow is Cherenkov light in the lucite.

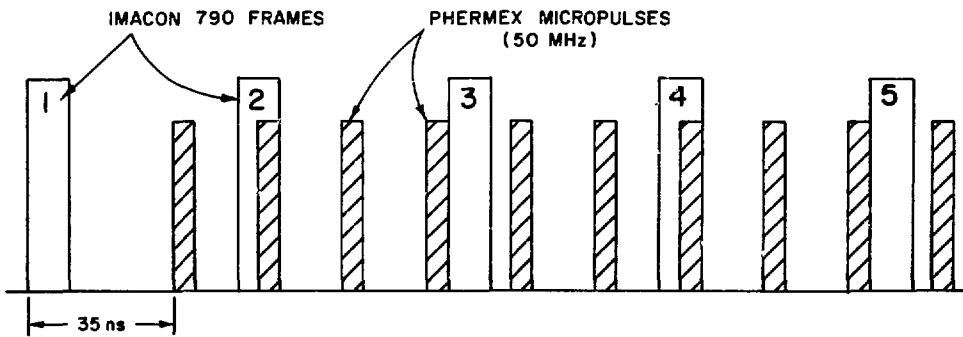
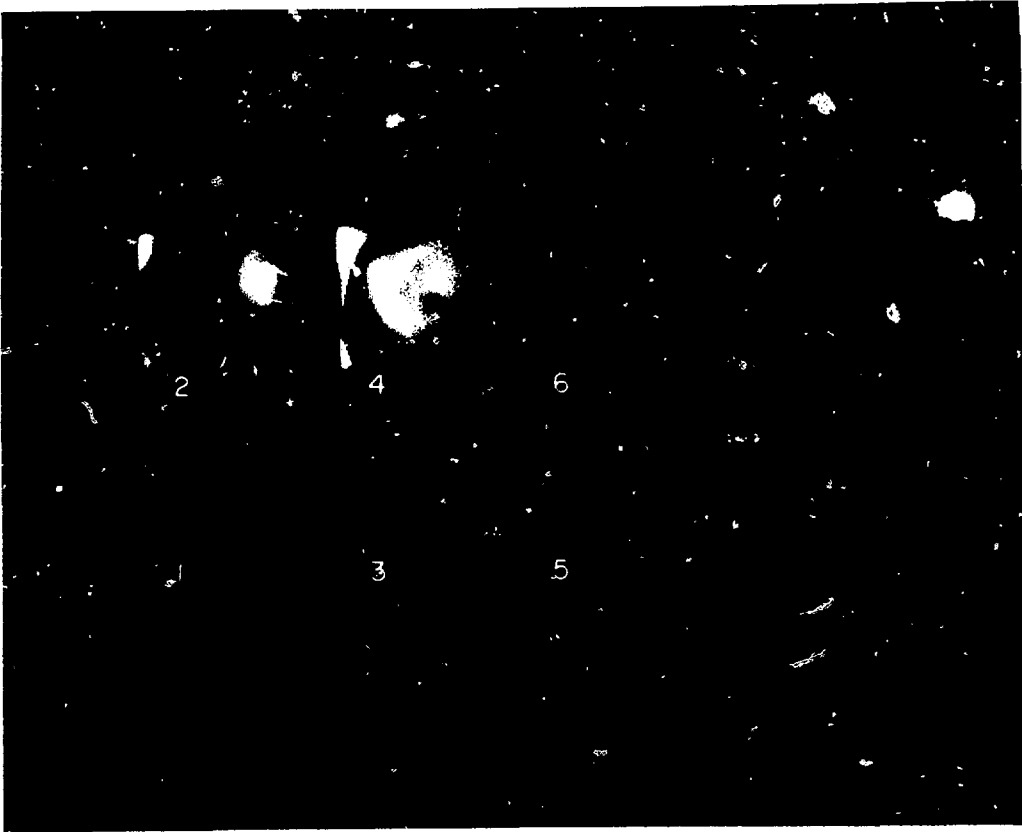


Fig. 9.

Imacon 790 fast frame record of the normal beam distribution 1.9 m from 1 mm focus for propagation in 3 torr neon. The overlay correlates the Imacon images with the beam microstructure. Relative timing was obtained using the NanoFast time digitizer.

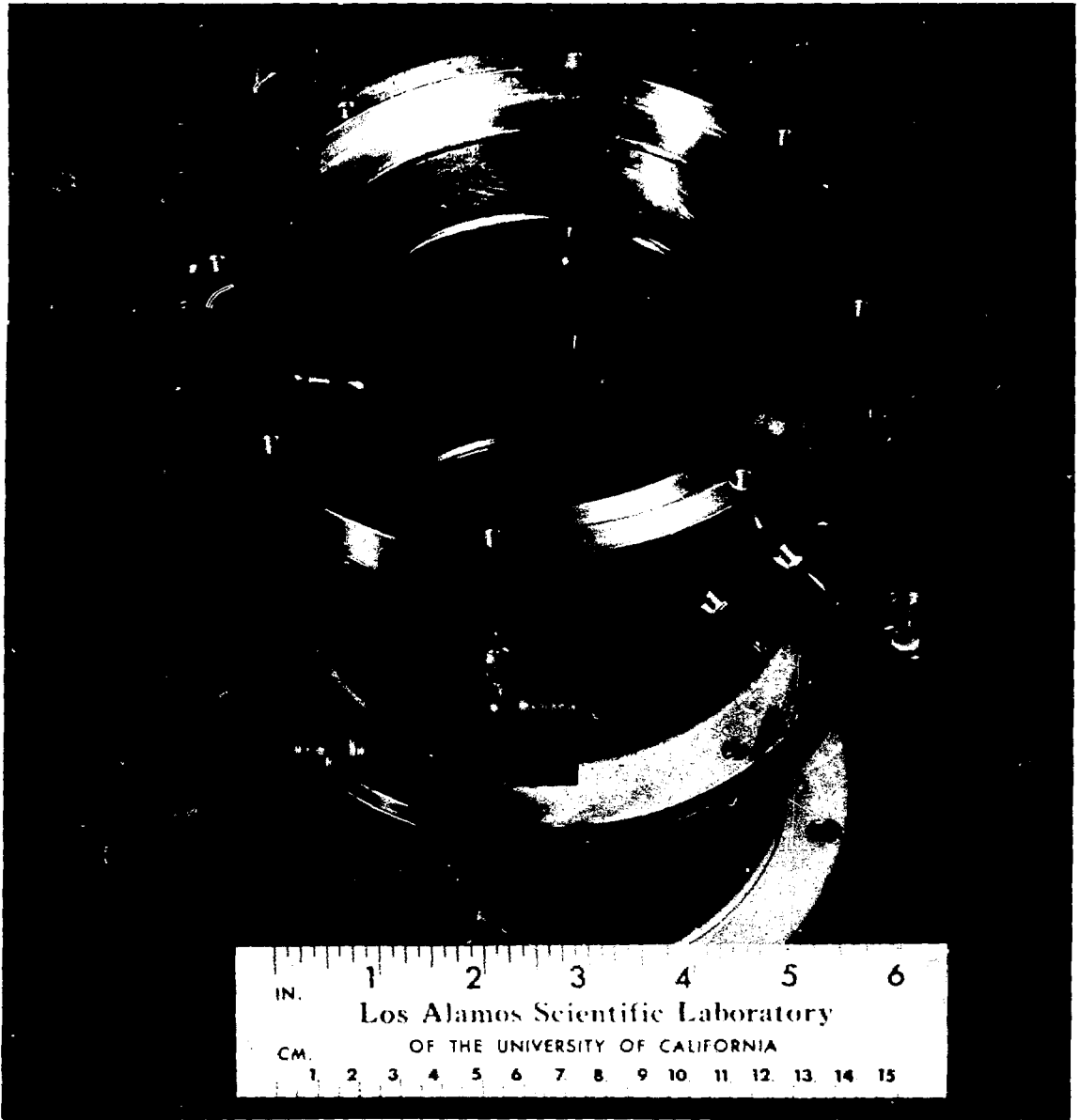


Fig. 10.

Photograph of drift tube segment containing the magnetic field probes used in the net current measurement. Probe areas are approximately 5 cm^2 .

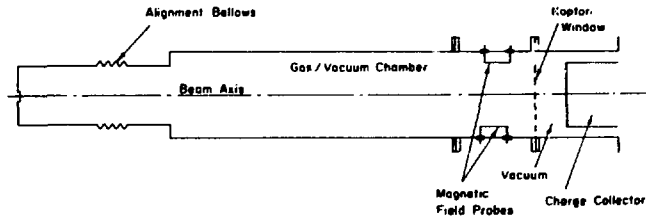


Fig. 11

Return-current measurement experimental arrangement. The charge collector is isolated by a kapton window to prevent collection of plasma current.

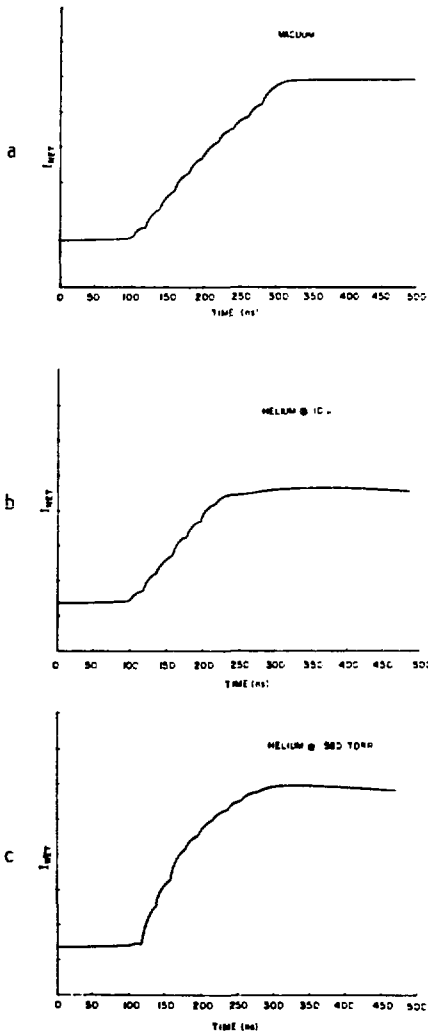


Fig. 12.

Net current in the drift tube as measured by magnetic field probes for (a) vacuum, (b) 10 μ helium, and (c) 580 torr helium.

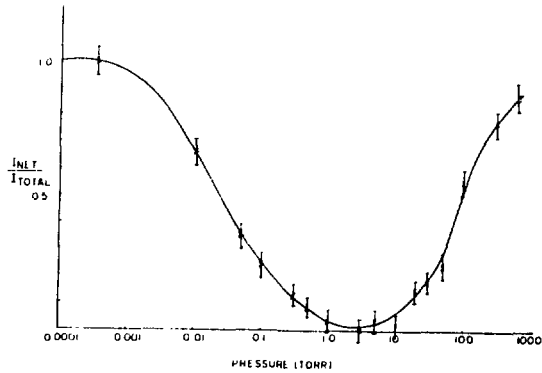


Fig. 13.

Ratio of the net current in the drift tube to the total propagated current as a function of pressure. The currents are integrated over the entire 200-ns macropulse.

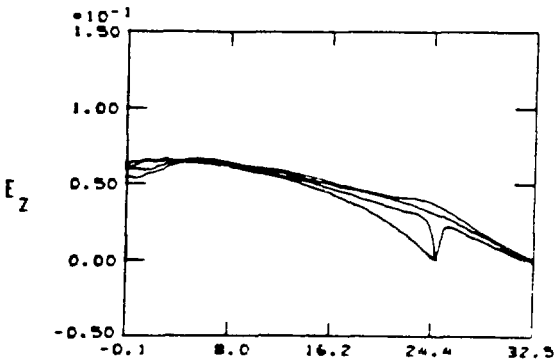


Fig. 14.

Radial profile of E_z cavity fields at four different z -positions (superimposed) at a given instant. Perturbation due to the antenna at $R = 25$ cm is clearly observable.

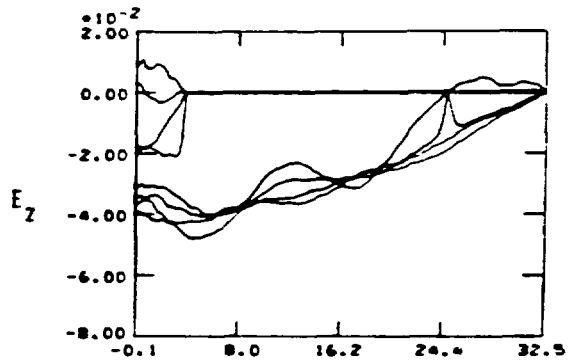


Fig. 15.

Radial profile similar to that in Fig. 14, except profiles of fringing fields are also included. Superposition of higher order cavity fields on the fundamental is evident.